Estimation of the Underlying Fiber Orientation Using Spherical k-means Method from the Diffusion ODF in HARDI Data

Huaizhong Zhang, Martin McGinnity, Sonya Coleman and Min Jing

Intelligent Systems Research Centre, University of Ulster at Magee,
Derry, BT487JL, Northern Ireland, UK
{h.zhang, tm.mcginnity, sa.coleman, m.jing}@ulster.ac.uk

Abstract. This paper presents a new approach for detecting the underlying fiber directions in a voxel. The main idea is to use the principal direction (centroid of orientation class) of an orientation population instead of the classical maximal direction of diffusion orientation density function (ODF) for fiber orientation. Firstly, diffusion orientations from the ODF of raw data have been classified in accordance with the expected fiber populations. The centroids of diffusion orientations are then determined using the spherical k-means method so as to estimate fiber orientations. The proposed method is based on the reconstruction of diffusion ODF using spherical harmonic (SH) decomposition and the characterization of diffusion anisotropy in a voxel. It can approximate fiber orientations accurately and avoid the spurious detection of fiber orientation which is often observed with traditional methods. By using a variety of synthetic, phantom and real datasets, the experimental results demonstrate the effectiveness of the proposed method.

Key words: HARDI, spherical k-means method, diffusion ODF, QBI

1 Introduction

In fiber orientation studies, high angular resolution diffusion imaging (HARDI) [1] has been recently proposed as an advance on Diffusion Tensor Imaging (DTI), to address concerns related to the presence of complex local geometries such as fiber crossings and intermixing of tracts. The main issue is that DTI assumes a single fiber direction in each voxel and fails to model complex microstructures. Various analytical methods for HARDI have been developed to capture fiber angular information and resolve non-trivial fiber configurations [1-2], particularly the diffusion orientation distribution function (ODF) reconstruction [3-5]. Tuch [5] proposed Q-ball imaging (QBI) for reconstructing the diffusion ODF of the underlying fiber populations by radially integrating the signal on the sphere using the Funk-Radon transform. Furthermore, the spherical harmonic decomposition has been successfully employed to obtain a robust ODF approximation at each voxel of the HARDI data [2, 6]. The local fiber orientation can then be inferred by computing the maxima of the diffusion ODF, because the correspondence between the peaks of the diffusion ODF and the principal directions of the underlying fibers has been established experimentally [4,

7]. Several methods exist to obtain the maxima of the ODF and estimate the fiber orientation, such as Powell's method [3], Newton-Raphson method [4] and high-order Cartesian tensor representation [8]. However, the estimation accuracy of fiber orientation is not only limited by parameter setting in the reconstruction algorithms, but the local maxima of the diffusion ODF [8, 9]. None of the representatives of the ODF function can currently present the true distribution of the fiber orientations and there is still ongoing research to investigate this problem [10]. In addition, the mapping between these quantities may be very complex so that it is difficult to find the fiber orientation if one solely depends on the maximal strategy. Thus, the estimates from the maxima of the diffusion ODF are likely to deviate from true fiber orientations. From a biological perspective, each single fiber bundle should coincide with an ODF peak of finite width, but these peaks could interfere in the joint ODF such as the crossing fiber case and thus the maxima of the resultant distribution would no longer correspond to the modes of the real peaks [11]. In QBI, such deviated direction estimation for an ODF function has been clearly addressed in [4, 9].

In fact, much of the information stored in diffusion ODF is neglected if we only use the maxima of diffusion ODF as fiber orientation estimations. Ideally one should make appropriate use of diffusion ODFs obtained by multiple fiber reconstructions for detecting the 'true' fiber orientations rather than simply taking the maximal direction. As an alternative to estimate dominant fiber orientations, spherical clustering should be useful to extract fiber orientation by exploiting global orientation information in diffusion ODF. In this paper we address these issues and the proposed method can be described as follows. The diffusion ODF of HARDI data is obtained firstly by applying the Q-ball imaging algorithm, which is a SH decomposition and a truncated SH series corresponding to the number of fiber populations (k) in a voxel [6, 14]. Then, we use the sampling orientations for calculating the ODF values on a sphere and set an approximate threshold for discarding the outliers. Thereafter, a set of orientations is presented that consists of distinct orientation clusters enclosing fiber orientations, and finally the spherical k-means method is applied to classify the orientation set into k classes and calculate the centroid of each class corresponding to each fiber. The rest of the paper is organized as follows. In Section 2, the proposed method and its implementation are discussed. The experimental results are presented in Section 3. Finally we conclude the paper and describe future work in Section 4.

2 The Proposed Method

2.1 Reconstruction of diffusion ODF

Recently, several analytical solution schemes have been proposed to implement the QBI algorithm with a SH basis [3-6], which addresses the HARDI signal as a SH series of order L. As the ODF is a real valued antipodally symmetric function, a modified SH basis of even order is designed to do the SH expansion. Based on the Funk-Hecke theorem and the Laplace-Beltrami regularisation, the desired regularised ODF can be reconstructed in the gradient direction (θ, φ) as in [6]:

$$\mathrm{ODF}(\theta,\varphi) = \sum_{j=1}^{R} 2\pi P_{l_j}(0) c_j Y_j \ (\theta,\varphi) \quad (1)$$

where c_j is the SH coefficient, $P_{l_j}(0) = (-1)^{\frac{l_j}{2}}(1 \cdot 3 \cdot 5 \cdots (l_j - 1)/(2 \cdot 4 \cdot 6 \cdots l_j))$, l_j is the order associated with the j^{th} element of the SH basis, and $R=(L+1)(L+2)/2$. Y_j is the j^{th} element in the modified basis Y.

In eq. (1), the robustness of the ODF needs to be ensured by choosing a proper order L of the SH expansion. The diffusivity in a voxel is usually determined from the order L of the SH expansion (isotropic: $L=0$, anisotropic Gaussian (single fiber), $L=2$, non-Gaussian (two fibers) $L=4$) [2]. In fact, the choice of the SH order and the number of fiber populations can be obtained by applying the method in [12].

2.2 Spherical k-means algorithm

Suppose we have n unit orientation vectors $\{x_1, x_2, ..., x_n\}$ in R^d. For these orientations, the inner product for any two orientations x and y can naturally be a similarity measure:

$$x^T y = \|x\|\|y\| \cos\theta = \cos\theta \quad (2)$$

where θ denotes the angle of two orientations. For partitioning these orientations $\{x_1,x_2,...,x_n\}$ into k disjoint classes $\pi_1, \pi_2, \ldots, \pi_k$ such that

$$\bigcup_{j=1}^{k} \pi_j = \{x_1, x_2, \ldots, x_n\} \text{ and } \pi_j \cap \pi_l = \emptyset \text{ if } j \neq l \quad (3)$$

for each fixed $1 \leq j \leq k$, the centroid of the orientations contained in the class π_j is

$$m_j = \frac{1}{n_j} \sum_{x \in \pi_j} x \quad (4)$$

where n_j is the number of orientations in π_j. The centroid is normalised as follows:

$$c_j = \frac{m_j}{\|m_j\|} \quad (5)$$

Thus, this normalised centroid can be used as the closest orientation to all the orientations in the class π_j using the cosine similarity in eq. (2). For measuring the quality of a given partitioning $\{\pi_j\}_{j=1}^{k}$, the following objective function is used:

$$\Psi\left(\{\pi_j\}_{j=1}^{k}\right) = \sum_{j=1}^{k} \sum_{x \in \pi_j} x^T c_j \quad (6)$$

By applying this objective function, the optimal solution of partitioning $\{x_1, x_2, ..., x_n\}$ into k disjoint classes $\pi_1^*, \pi_2^*, \ldots, \pi_k^*$ can be described as the following problem:

$$\{\pi_j^*\}_{j=1}^{k} = \mathrm{argmax}_{\{\pi_j\}_{j=1}^{k}} \ \Psi\left(\{\pi_j\}_{j=1}^{k}\right) \quad (7)$$

However, the above problem is NP-complete and the optimal solution cannot be obtained analytically. Dhillon [13] presented an approximation algorithm for this problem, namely the spherical k-means algorithm, can be summarised as follows:

(1) Give an initial partitioning of the orientations, namely $\{\pi_j^{(0)}\}_{j=1}^{k}$. Let $\{c_j^{(0)}\}_{j=1}^{k}$ denote the centroids associated with the given partitioning. Set the index of iteration $t=0$.

(2) Compute the new partitioning $\{\pi_j^{(t+1)}\}_{j=1}^{k}$ based on the previous centroids $\{c_j^{(t+1)}\}_{j=1}^{k}$:

$$\pi_j^{(t+1)} = \left\{x \in \{x_i\}_{i=1}^{n} : x^T c_j^{(t)} > x^T c_l^{(t)}, 1 \leq l \leq k, l \neq j\right\}, 1 \leq j \leq k.$$

(3) Compute the new centroids:

$$c_j^{(t+1)} = m_j^{(t+1)} / \left\| m_j^{(t+1)} \right\|, 1 \le j \le k,$$

where $m_j^{(t+1)}$ is the centroid of class $\pi_j^{(t+1)}$.

(4) If $|\Psi\left(\left\{\pi_j^{(t+1)}\right\}_{j=1}^{k}\right) - \Psi\left(\{\pi_j^{(t)}\}_{j=1}^{k}\right)| \le \epsilon$, the iteration stops. Otherwise, $t = t + 1$, and go to step 2.

2.3 Proposed method for calculating the underlying fiber orientation

Based on the QBI techniques in [5-6] and the method in [12], fiber populations are firstly detected in a voxel. Then the spherical k-means method is employed to obtain the centroid of the orientation class to represent the underlying fiber orientation. The implementation procedure is described as follows:

(1) The ODF is reconstructed using the SH decomposition based on QBI.
(2) The number of fiber populations, k_c, is obtained by applying the method proposed in [12]. In this step, the order L of the truncated SH decomposition is obtained by minimising the information entropy of the initial SH decomposition.
(3) The distributed dataset S of the ODF's values in various orientations is produced, by which a high angular resolution orientation scheme such as 755 orientations is employed.
(4) A threshold T is used for filtering the dataset S and alleviating the affects of noise. Thus, a new set of discrete ODF values, S_u, is obtained and a set of orientations, O, is obtained according to the set S_u.
(5) O is classified into k_c classes by applying the spherical k-means and the centriods are calculated.

In addition, to better improve the performance, we choose the threshold larger than 0.7 and keep the number of class member is at least 20.

3 Experimental Results

3.1 Application in synthetic data

Synthetic data are generated using the multi-tensor model with 61 gradient directions and b=1500 s/mm^2. In the experiments, the maxima of diffusion ODF are calculated by applying the gradient ascent method with a discrete strategy as introduced in [14]. Considering the approximation process of the conventional analytical methods [3, 4] being limited to the mesh size and sensitive to local maxima, the overall performance of this discrete strategy is better than that of analytical solution both in simplicity and efficiency. Thus, we will compare the proposed method with the discrete gradient ascent method (named as the traditional method) in the following experiments.

Figs. 1(a-e) show five voxel datasets containing a single fibre with the azimuthal angles 10°, 20°, 30°, 40°, 50° (polar angle=90° for all) respectively. The dotted arrow is the estimated orientation and the solid arrow is the actual fibre orientation. The numerical results are presented in Table 1. Columns, estimation, bias_e, maximum, bias_m and fibre denote the estimated orientation, the estimated bias, the maximal orientation, the bias of maximal orientation and the fibre orientation respectively. It can be seen that the performance of the estimated orientations using the proposed method is better than that of the maximal orientations using the traditional method. For example, the estimated orientation, (0.937, 0.348, -0.002), for the 20° dataset only has 0.402° bias from the fibre orientation, (0.940, 0.342, 0.000), but the maximal orientation, (-0.928, -0.370, -0.040), is 2.867° deviating from the fibre.

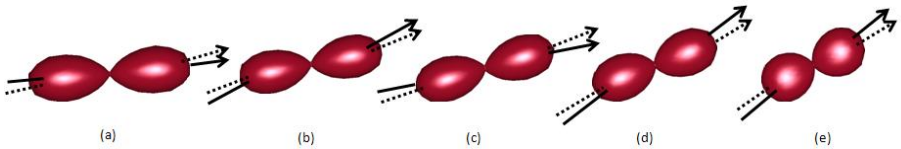

Fig. 1 Visualization of five datasets of single fibre with various orientations. (a) – (e) are the datasets with $10^{\circ}-50^{\circ}$ rotation angles in which the dotted arrow is the estimated orientation and the solid one is the fibre.

Table 1 Estimation results applying the proposed method in single fibre datasets

voxel	Estimation	bias_e	Maximum	bias_m	Fibre
10°	0.985 0.170 -0.010	0.631	0.992 0.129 -0.004	2.623	0.985 0.174 0.00
20°	0.937 0.348 -0.002	0.402	0.928 0.370 0.040	2.867	0.940 0.342 0.00
30°	0.859 0.511 0.008	0.871	0.878 0.479 0.004	1.412	0.866 0.500 0.00
40°	0.764 0.645 0.010	0.587	0.727 0.687 0.004	3.398	0.766 0.643 0.00
50°	0.638 0.770 0.010	0.685	0.639 0.769 0.040	2.312	0.643 0.766 0.00

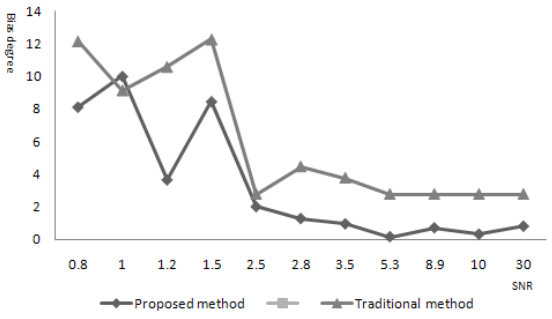

Fig. 2. Performances of the proposed method and the traditional method in the datasets with different SNR levels.

For examining the robustness in noisy situation, we applied the proposed method to the generated one-fibre datasets with different noise levels. Fig. 2 illustrates the results using the proposed method and the traditional method respectively, which shows that the overall performance of the proposed method is better and more robust. Due to generating the noisy data randomly, the performances of the two methods are fluctuated over the datasets.

Table 2 Estimation results applying the proposed method in crossing fibre datasets

Voxel	estimation	bias_e	angle_e	fibre
10°	c1: 0.950 0.001 0.08 c2: 0.979 0.197 -0.049	0.45 3.13	11.74	f1: 1 0 0 f2: 0.985 0.174 0
20°	c1: 1.0 0.01 -0.002 c2: 0.939 0.344 -0.025	0.60 1.43	19.61	f1: 1 0 0 f2: 0.940 0.342 0
30°	c1: 1.0 0.030 -0.027 c2: 0.869 0.494 0.020	2.31 1.19	28.05	f1: 1 0 0 f2: 0.876 0.50 0
40°	c1: 0.998 0.030 -0.053 c2: 0.774 0.632 0.040	3.49 2.45	37.88	f1: 1 0 0 f2: 0.766 0.643 0
50°	c1: 1.0 0.001 -0.041 c2: 0.691 0.722 0.014	2.36 3.83	46.30	f1: 1 0 0 f2: 0.643 0.766 0

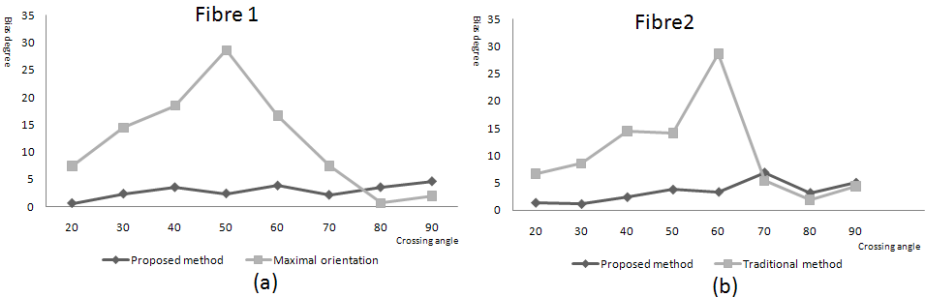

Fig. 3. Comparison of the proposed method and the traditional method by applying them in the datasets with crossing angles 20°, 30°, 40°, 50°, 60°, 70°, 80°, 90°. Here the gradient scheme is 755 directions. (a) is the bias of the estimated orientation for fibre 1. (b) is the bias of the estimated orientation for fibre 2.

We use the datasets of crossing fibres to further demonstrate the effectiveness of the proposed method. Five generated diffusion datasets have different crossing angles of two fibres from 10° to 50°, which Hess [14] pointed out that the traditional methods is incapable of resolving the cases of crossing fibers appropriately when the crossing angle is less than 65°. The results using the proposed method are presented in Table 2. The columns, estimation, bias_e, angle_e and fibre denote the estimated orientations, the estimated biases, the crossing angle of two estimated orientations and the ground truth respectively. Table 2 shows that the estimates of fibre orientations are accurate although its overall performance is inferior to that of one fibre cases in Table 1. Generally, we can estimate the crossing angle quite well when we consider the absolute bias, |estimation – fibre angle|, such as 1.74°, 0.39° for the 10°, 20°

datasets respectively. The relative bias, |estimation – fibre angle|/fibre angle, seems to be unsatisfactory for some datasets, for example it is 17.4% for the 10° case. However, the estimation bias will be significant if we use the maximal orientations as the estimated fibre orientations. For example, in the dataset with 40° crossing angle, the maximal orientations are m1=(0.932, 0.355, -0.080) and m2=(0.999, 0, 0.034), the absolute biases are 1.94° and 19.68° respectively and the estimated crossing angle is only 21.84°. In contrast, the estimated orientations using the proposed method are c1=(0.998, 0.030, -0.053) and c2=(0.774, 0.632, 0.040), the absolute bias are 3.49° and 2.45° respectively, and the estimated crossing angle is 37.88°. Fig. 3 illustrates the estimated accuracies (absolute bias) by applying these two methods in a series of datasets with crossing angles 20°, 30°, 40°, 50°, 60°, 70°, 80°, 90°. Fig. 3(a) and Fig. 3(b) show the results for the first fibre and the second fibre respectively. For the cases of less than 70°, the estimation using the traditional method deviates from fibre orientation significantly and often leads to large bias, which corresponds to the angle assumption discussed in [14]. It can be seen that the proposed method performs much better and the overall bias is at a low level. On the other hand, in the cases of more than 70°, the performance of the traditional method is improved significantly and is slightly better than that of the proposed method.

3.2 Application in phantom data

Phantom data has ground truth which can help examine the proposed method. The fibercup phantom dataset [15] was acquired using 64 diffusion gradients and one baseline, which has 3 slices, each slice with a resolution of $3*3*3mm^3$, NEX=2 and b-value=$1500smm^{-2}$. Fig. 4(a) shows the ground truth of the dataset and Fig. 4(b) presents the voxel classification result using the method proposed in [12] (Dark gray: isotropic, light gray: Gaussian, white: non-Gaussian). The proposed method is applied in this dataset, which the threshold is 0.9 for Gaussain case and 0.75 for non-Gaussian case. Fig. 4(c) visualizes the result of the obtained fiber orientations in that the color scheme indicating orientation is the same as in DTI (red: left-right, green: anteroposterior, blue: superior-inferior) and the background (gray level) of each grid corresponds to the generalized fractional anisotropy (GFA) value in each voxel. In contrast to the ground truth, the overall fiber orientations can be well estimated by the proposed method. Fig. 4(d) shows two enlarged ROIs highlighted in Fig. 4(c). One ROI is at the corner of the fiber U-shape that the enlarged image shows the orientation tendency. Another one shows the ROI with two parallel fibers that the acquired orientations can preserve the fiber orientation well. Note that the color indicates partially anteroposterior direction because the second slice is selected for calculation and the fiber orientation can lead to the third slice due to the acquired signals.

3.3 Application in real data

The real dataset was acquired from a healthy volunteer on a 1.5T GE Signa Excite scanner, which the EP/SE sequence parameters include $b=1.1477\times109sm^{-2}$, $\delta=0.034s$, $\Delta=0.04s$, $TE=0.087s$, $G=0.022Tm^{-1}$, 55 DW directions, voxel size $3\times3\times3mm^3$, 30 slices with an acquisition matrix 128×128 interpolated to 256×256. The data was granted for use in this study by CCSBS/UAF. It is anatomically known that there exist various fibre tracts in the regions of the corpus callosum such as rostrum, genu,

truncus, isthmus and splenium [16]. Thus, we choose the ROI (the highlighted inset in Fig. 5(a)) for demonstrating the performance of our method, which is part of the genu

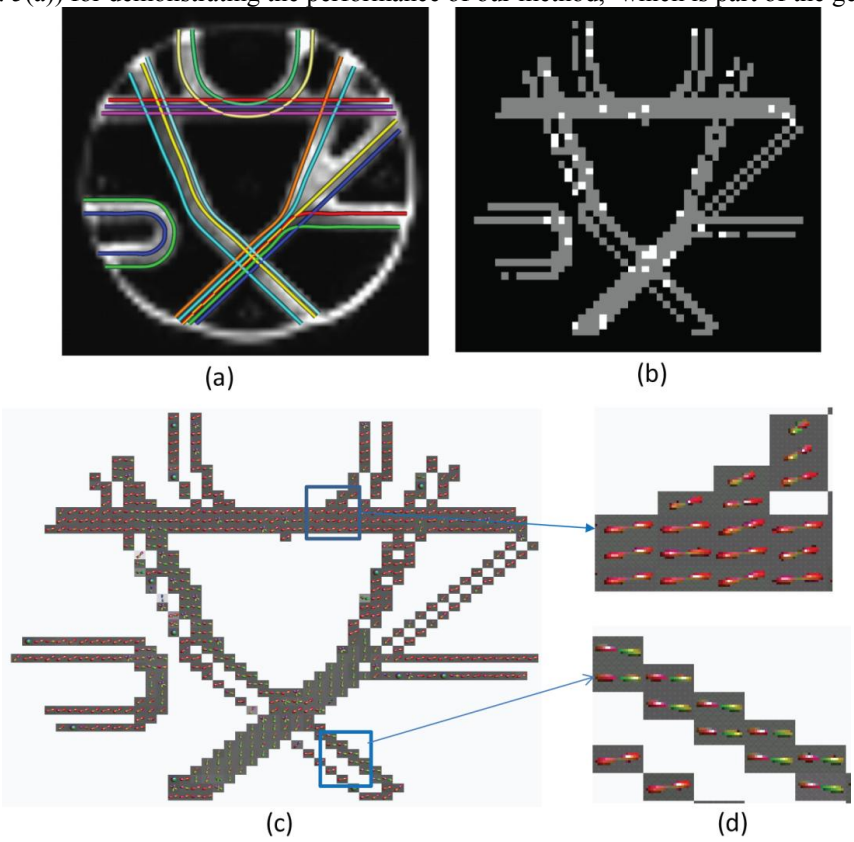

Fig. 4. Result for a phantom datset. (a) is the ground truth, (b) is the voxel classification result, (c) is the visualised result using the proposed method and (d) presents the enlarged ROIs in (c).

and the subregion [43:50,120:135] in the original acquired image. Fig. 5(a) shows the acquired image with a gradient. Fig. 5(b) is the result map of voxel classification of the ROI using the method in [12] (light gray: Gaussian, one fiber; white: non-Gaussian, two fibers). We visually present the results using the proposed method in Fig. 5(c), which applies the color scheme of DTI to indicate orientation. The fibre orientation (ODF) in each voxel is superimposed on a grayscale background modulated by the GFA in that voxel (black:GFA=0;white:GFA=1). It is shown that the fibre population in the ROI has an obvious orientation tendency that is consistently with the anatomical knowledge of the fibre tracts in the genu of the corpus callosum, in which the thinner axons connect the prefrontal cortex between the two halves of the brain. In addition, the splenium of the corpus callosum is situated dorsal to the pineal body, which consists of fascicles of myelinated fibers. In addition, we apply the proposed method in the ROI of the splenium (Fig. 5(d), [120:125, 126:135] in slice 6), which the GFA range is [0.3257, 0.5236]. Fig. 5(e) is the result

map of voxel classification (light gray: Gaussian, one fiber). Fig. 5(f) visualises the result of the ODF in this ROI and the fiber orientations are clearly consistent with the anatomical information of fascicles of fibers in the splenium.

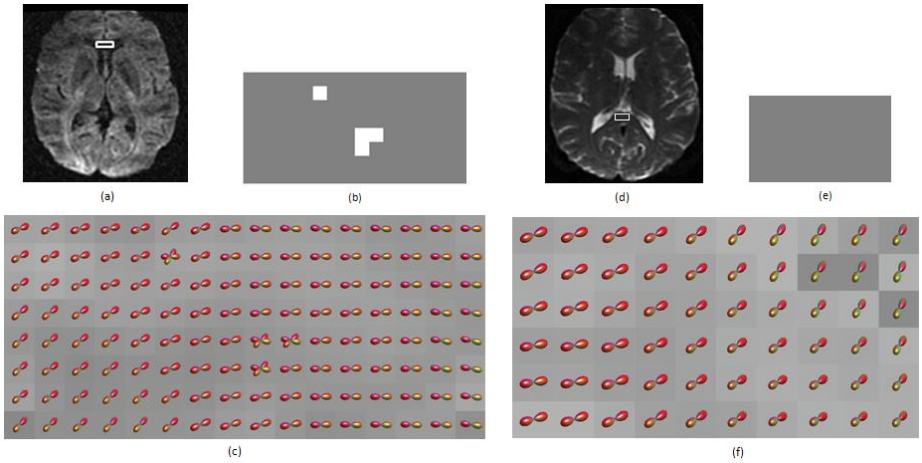

Fig. 5. (a) slice 4 with diffusion gradient, the highlighted ROI (8*16) is part of Genu; (b) voxel classification results in the highlighted ROI in (a) (light gray: single fibre; white: two fibres); (c) visualisation of the ROI's ODFs derived from the proposed method. (d) slice 6 (b0), the highlighted ROI (6*10) is part of splenium; (e) voxel classification results in the highlighted ROI in (d); (f) visualisation of the ROI's ODFs. The ODF in each voxel is superimposed on a grayscale background modulated by the GFA in that voxel (black: GFA=0; white: GFA=1).

4 Conclusions

The proposed method aims to accurately estimate fiber orientations using information on orientation classes, so as to recover fiber orientations. There are two major advantages of the proposed method. First, the proposed method can make sufficient use of the orientation information in diffusion ODF, because there is usually a set of principal diffusion orientations concentrating around the fiber orientation as disclosed in a fibrous voxel; secondly, the proposed method can avoid the risk of solely depending on insufficient information for fiber orientation detection, such as local maxima in traditional methods; particularly, the proposed method can be applied to the cases with low crossing angle which the traditional methods fail to detect the orientations [14].

However, some limitations exist in the proposed method. Firstly, this is a discrete numerical solution and it needs to set the threshold and use a high angular resolution gradient scheme. Secondly, the choice of a threshold is a key factor in the solution scheme because an appropriate one can alleviate the affects of noise and artefacts in clustering process. Considering this threshold problem, we apply an average strategy to improve the performance of the algorithm. However, this strategy can only obtain a quasi-optimal solution rather than an optimal one. Future work will use three

approaches to improve this proposed method. Firstly, considering the above limitations, we will apply some higher angular resolution gradient schemes for improving the estimation accuracy. Secondly, we need to incorporate some anatomical information of the ROIs into the solution scheme so as to improve the performance. Finally, we can employ other ODF reconstruction schemes such as the spherical deconvolution in the solution scheme.

References

1. Tuch, D., Reese, T., Wiegell, M., Makris, N., Belliveau, J., Wedeen, V.: High angular resolution diffusion imaging reveals intravoxel white matter fiber heterogeneity. Magn. Reson. Med., 48:577-82(2002)
2. Frank, L.: Characterization of anisotropy in high angular resolution diffusion-weighted MRI. Magn. Reson. Med., vol.47(6):1083-1099(2002)
3. Jansons, K., Alexander, D.: Persistent angular structure: new insights from diffusion magnetic resonance imaging data. Inverse Problems, 19:1031-46(2003)
4. Tournier, J., Calamante, F., Gadian, D., Connelly, A.: Direct estimation of the fiber orientation density function from diffusion-weighted MRI data using spherical deconvolution. NeuroImage, 23:1176-1185(2004)
5. Tuch, D.: Q-ball imaging. Magn. Reson. Med., vol.52:1358-72(2004)
6. Descoteaux, M., Angelino, E., Fitzgibbons, S., Deriche, R.: Regularized, fast, and robust analytical Q-ball imaging, Magn. Reson. Med., 58:497-510(2007)
7. Perrin, M., Poupon, C., Rieul, B., Leroux, P., Constantinesco, A., Mangin, J., Lebihan, D.: Validataion of Q-ball imaging with a diffusion fiber-crossing phantom on a clinical scanner. Philos. Trans. R. Soc. Lond. B. Biol. Sci. 360(1457): 881-91(2005)
8. Bloy, L., Verma, R.: On computing the underlying fiber directions from the diffusion orientation distribution function. MICCAI 2008, Part I, LNCS 5241, pp. 1-8(2008)
9. Zhan, W., Yang, Y.: How accurately can the diffusion profiles indicate multiple fiber orientations? A study on general fiber crossings in diffusion MRI. Journal of Magnetic Resonance, 183:193-202(2006)
10. Tristan-Vega, A., Westin, C., Aja-Fernandez, S.: A new methodology for the estimation of fiber populations in the white matter of the brain with the Funk-Radon transform. NeuroImage 49:1301-15(2010)
11. Schultz, T., Seidel, H.: Estimating crossing fibers: a tensor decomposition approach, IEEE Trans. Visualization and Computer Graphics, vol. 14(6):1635-1642(2008)
12. Zhang, H.Z., McGinnity, T.M., Coleman, S., Jin, M.: A novel criterion for characterizing diffusion anisotropy in HARDI data based on the MDL technique. Proceedings of ICMB 2010, Hong Kong, China(2010)
13. Dhillon, I.S., Modha, D.S.: Concept decompositions for large sparse text data using clustering. Machine Learning, 42: 143-175(2001)
14. C. Hess, P. Mukherjee, E. Han, D. Xu and D. Vigneron. Q-ball reconstruction of multimodal fiber orientations using the spherical harmonic basis, Magnetic Resonance in Medicine, 56:104-117(2006)
15. Fillard, M. Descoteaux, A. Goh, S. Gouttard, B. Jeurissen, J. Malcolm, A. Ramirez-Manzanares, M. Reisert, K. Sakaie, F. Tensaouti, Yo T, J. Mangin, C. Poupon. Quantitative evaluation of 10 tractography algorithms on a realistic diffusion MR phantom. Neuroimage 56(1):220-34(2011)
16. M.R. Wiegell, H. Larsson and V.J. Wedeen. Fiber crossing in human brain depicted with diffusion tensor MR imaging. Radiology 217(3):897-903(2000)